WDS'14 Proceedings of Contributed Papers — Physics, 227–232, 2014. ISBN 978-80-7378-276-4 © MATFYZPRESS

Parallel Heat Flux Decay Length Study in the COMPASS Tokamak Using MWIR and LWIR Cameras

P. Vondráček, J. Horáček, R. Pánek

Institute of Plasma Physics AS CR, Prague, Czech Republic.

E. Gauthier

CEA/DSM/IRFM, CEA Cadarache, Saint-Paul-lez-Durance, France.

Abstract. A comprehensive study of a parallel heat flux in a tokamak scrape-off layer (SOL) has been performed in the COMPASS tokamak recently. Specially shaped high field side (HFS) limiter was used to estimate a heat flux radial decay length for small limiter radial misalignment.
Long wavelength IR microbolometer and medium wavelength IR InSb camera were used for this purpose. This paper compares results obtained by the means of both cameras and demonstrates observation of very narrow heat flux decay length close to the last closed flux surface (LCFS) independantly on used camera.

Introduction

Unexpected power load near the LCFS on tokamak high field side inner wall limiters has been observed recently [*Arnoux et al.*, 2013]. A narrow *parallel heat flux characteristic decay length* (λ_q) is thus expected to be present in the near scrape-off layer. Such narrow SOLs were not reflected in the design of the ITER first wall (FW) panels, which are shaped to spread the heat flux homogeneously to a large surface and protect against misalignments. A detailed study of the near-SOL heat flux was consequently performed in the COMPASS tokamak [*Horacek et al.*, 2015] and partially also in the TCV [*Nespoli et al.*, 2015] and DIIID tokamaks [*Stangeby et al.*, 2015].

Special HFS limiters experiments in the COMPASS tokamak

A series of dedicated experiments has been performed in the COMPASS tokamak [*Panek et al.*, 2006], in which specially designed inner wall graphite limiters have been installed at a single toroidal location on the central column. One of these limiters was so-called recessed roof-shaped limiter with two apexes simulating ITER continuous HFS limiter with small misalignments. Radial position of the limiter was varied compared to the rest of the central column during the experimental campaigns to study near-SOL dependence on the limiter misalignment. Data presented in this paper describes limiter inserted 4 mm into the plasma compared to the neighboring tiles.

Temperature distribution over the limiter was measured using infrared (IR) camera located at a low field side (LFS) midplane radially approx. at a distance of 1 m from the limiter. Two different IR cameras with independent calibration and different wavelength sensitivity were used to compare the results.

The limiter heat load distribution was calculated from the temperature signal using the THEODOR code [*Herrmann et al.*, 1995]. The required radial profiles of a parallel heat flux in a SOL were extracted using EFIT reconstruction of magnetic surfaces (calculating magnetic field line incidence angle and distance to the LCFS for each pixel). Various magnitudes and directions of plasma currents were used to study near-SOL variation with an ohmic heating power.

The results shown in this paper have been used to determine the near-SOL feature presented by *Horacek et al.* [2015]. In order to explain the near-SOL feature, effect of non-ambipolar plasma conditions at the limiter surface was studied by *Dejarnac et al.* [2015] demonstrating its importance, however not a dominant role. It was demonstrated by *Horacek et al.* [2015] that the so-called heuristic drift-based model [*Goldston*, 2015] describes well the observed near-SOL feature, with a predictive capability for the ITER tokamak, which is currently under construction.

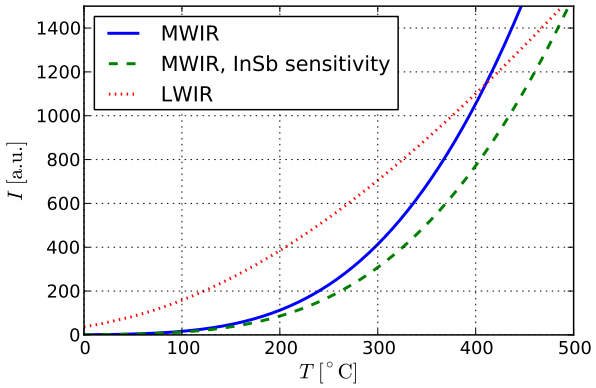

Figure 1. Illustration of the non-linear dependence of the radiation intensity on the black body temperature for MWIR and LWIR regions.

IR thermography

The COMPASS tokamak is equipped with the *Micro-Epsilon TIM160* camera. A detector of the camera is uncooled microbolometer with 160×120 px. and frame-rate 120 Hz. The detector is sensitive for a long wavelength IR radiation (LWIR) 7.5–13 μm. Four different temperature ranges could be used — altogether covering region from −20 °C up to 1500 °C. 35.5 mm lens with $6° \times 5°$ field of view (FOV) and 1 px. $\approx$ 1 mm was used.

Jade MWIR camera with an InSb detector was loaned for this experiment from CEA Cadarache. This detector is sensitive for a medium wavelength IR radiation (MWIR) in the range 3–5 μm, has 320 × 240 px. and can acquire data with a frame rate 50 Hz. Various temperature ranges can be achieved using different integration times (IT) and wavelength filters. 50 mm lens giving 1px. $\approx$ 0.6 mm was used.

Camera calibration

LWIR camera provided output directly in temperature values calibrated using calibration black body (see *Ulicny* [2013] for more details). Correction for germanium vacuum window transmissivity (τ) and graphite limiter emissivity (ε) were performed using camera software TIM Connect, which also automatically compensates results for the current ambient temperature (entering the measurement thanks to reflections from the vacuum window and from the limiter). Both values τ and ε were measured observing heated limiter with calibrated sticker ($\varepsilon = 0.95$). Measurement were performed for temperature range 20–200 °C, where $\tau \approx 0.87$ and $\varepsilon \approx 0.84$ were found.

MWIR camera data were stored in raw format (digital levels, DL). Detector provides 14 bit digital output, that is nearly linear function of incoming radiation intensity (I). Transformation of the detector DL output to radiation intensity was performed to incorporate all necessary signal corrections for e.g. vacuum window transmission and limiter emissivity. Radiation intensity to temperature transformation and vice versa was calculated by integration of Planck's law weighted by the detector sensitivity $S(\lambda)$ over the filter wavelength band

$$I(T) = \int_{\lambda_1}^{\lambda_2} \frac{2hc^2}{\lambda^5} \frac{1}{e^{\frac{hc}{\lambda k_B T}} - 1} S(\lambda) d\lambda. \tag{1}$$

Linear increase of the detector sensitivity $S(\lambda)$ from 55 % to 90 % over the range 3–5 μm was assumed as an approximate InSb detector sensitivity [*JEDEC*, 1969; *Rogalski*, 2010] because exact sensitivity for this particular detector was not available. Radiation intensity dependence on temperature for MWIR and LWIR regions (for $S(\lambda) = 1$) is shown in Figure 1 as well as the dependence with the correction for the InSb detector sensitivity.

Calibration I to DL dependence was fitted by the second order polynomial for each used integration time as the detector response was observed to be sligtly non-linear mainly for low radiation intensities. Measured dependence of the detector response on the radiation intensity and temperature for 3 ITs is shown in Figure 2.

Germanium vacuum window correction function ϕ in the range 3–5 μm as a function of a temperature of an observed object (black body) is shown in Figure 3. This function describes radiation attenuation

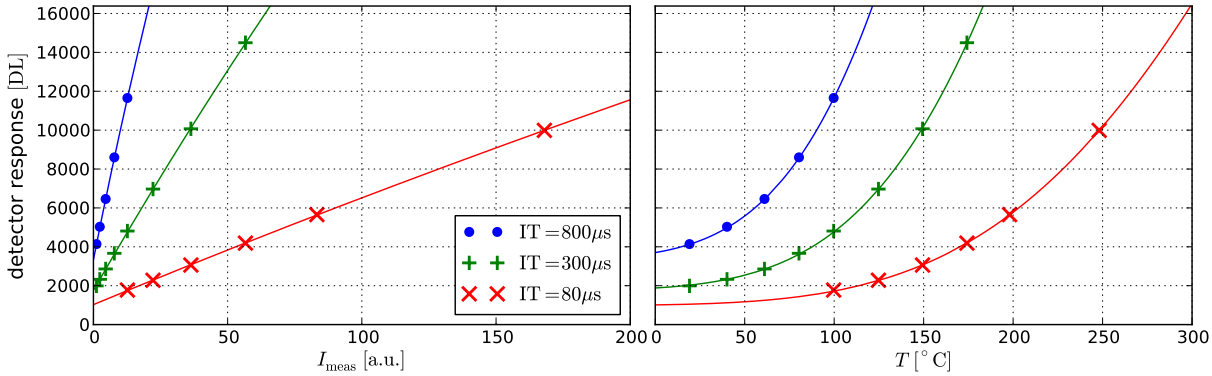

Figure 2. MWIR camera calibration: detector response as a function of temperature of a calibration black body (right) and corresponding radiation intensity corrected for the detector sensitivity (left).

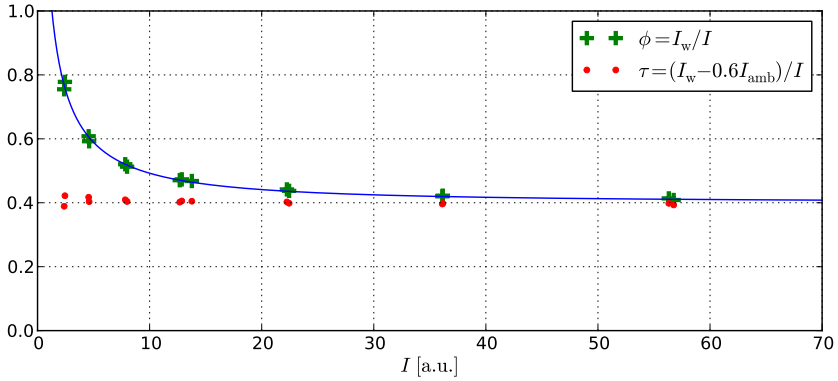

Figure 3. MWIR camera calibration: Germanium window correction function describing an attenuation of a radiation passing the window and reflection of an ambient radiation (green) and window transmissivity (red) — both as a function of a radiation intensity measured without the window.

inside the window together with a reflection of an ambient radiation emitted by the camera itself and its surroundings (at stable ambient temperature). It corresponds to the ratio of the radiation intensity measured by the camera with (I_w) and without (I) Ge window. Pure window transmissivity τ could be extracted from this function by subtraction of intensity of reflected ambient radiation (I_{amb}) from the radiation intensity measured by the camera — see Figure 3. Window transmissivity $\tau \approx 0.4$ was measured assuming ambient temperature $T_{amb} = 25$ °C and zero emissivity of the window.

Limiter emissivity was found to be $\varepsilon \approx 0.92$ for the radiation wavelengths 3–5 μm.

Measured signal transformed to radiation intensity was consequently translated to temperature using formula

$$T_{lim}(x,y,t) = I^{-1}\left(\frac{1}{\phi\left(I_w\right)\varepsilon} I_w(x,y,t,\mathrm{DL},\mathrm{IT}) - \frac{1-\varepsilon}{\varepsilon} I\left(T_{amb}\right)\right), \tag{2}$$

involving all the corrections mentioned above.

Multi-IT regime was used — MWIR camera collected data at 150 Hz with 3 different integration times and provided output at 50 Hz with automatically selected optimal IT for each pixel.

Heat flux calculation

The heat load associated with each pixel $q_{lim}(x,y,t)$ was derived from $T_{lim}(x,y,t)$ using the non-linear finite difference code THEODOR [*Herrmann et al.*, 1995]. The surface temperature measurements are affected by the presence of deposited layers [*Andrew et al.*, 2003][*Gauthier et al.*, 2005]. The thermal behavior of deposited layers has to be taken into account during the heat flux calculation. A heat transmission coefficient α of the surface layer is thus integrated into the THEODOR code [*Herrmann*, 2001]. It represents ratio of heat conductivity to thickness of the surface layer:

$$\alpha \equiv \kappa_{sl}/d_{sl}. \tag{3}$$

Limiter heat load is then

$$q_{lim} = \alpha \Delta T, \tag{4}$$

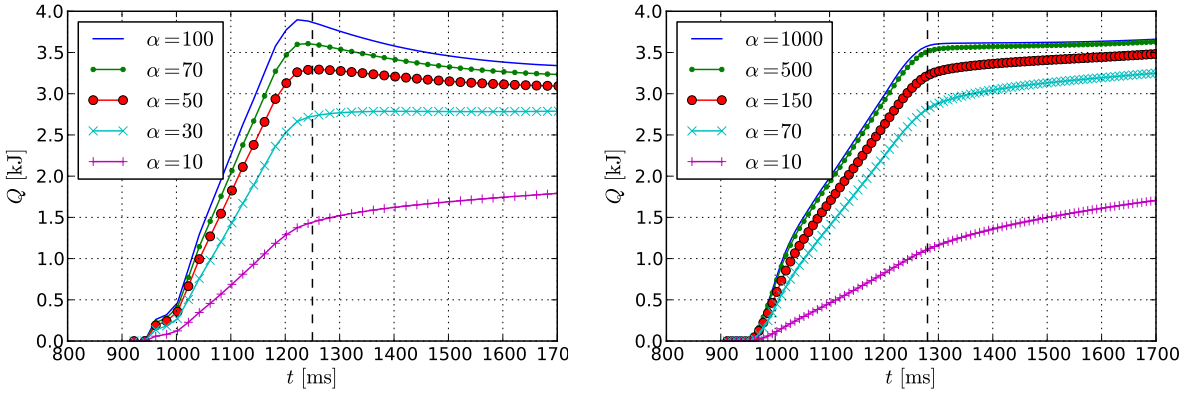

Figure 4. Stored energy in the observed limiter region for different assumed surface layer heat transmission coefficients α [kW·m^{-2}·K^{-1}] — left for MWIR camera (shot ♯7236), right for LWIR camera (shot ♯7266). Vertical dashed line indicates the end of the discharge.

where ΔT is the temperature difference between the top surface of the layer and the tile itself.

Heat transmission coefficient value could be estimated from the time evolution of the total energy stored in the limiter tile, which should remain constant after the plasma shot [*Lott et al.*, 2005]. Stored energy for different α values is shown in Figure 4. $\alpha = 50$ kW·m^{-2}·K^{-1} was used for the MWIR camera and $\alpha = 150$ kW·m^{-2}·K^{-1} for the LWIR camera.

The difference in the α values for both cameras is given probably mainly by the effect of micro hot spots (dust particles, surface roughness) acting in a similar way as the deposited surface layer [*Herrmann*, 2005; *Hildebrandt et al.*, 2005; *Delchambre et al.*, 2009]. IR detector provides mean value of the radiation intensity emitted by the area observed by each pixel. Temperature is thus overestimated (compared to the temperature mean value over the pixel area) thanks to its non-linear dependence on the radiation intensity. This effect is stronger for the MWIR range compared to the LWIR, where I to T relation is closer to the linear one as is shown in Figure 1. Discrepancy of temperature measurement in MWIR and LWIR range was investigated e.g. at the MAST tokamak and published by *Temmerman et al.* [2010] and *Delchambre-Demoncheaux et al.* [2011].

Note that the higher is the α value the lower is the correction for the surface layer.

Experimental results

Final radial profiles of the parallel heat flux in the SOL for 4 different plasma currents are shown in Figure 5. MWIR and LWIR measurements are compared for all I_p. The profiles could be fitted by the double-exponential function

$$q_\parallel(\Delta r) = q_{0,\mathrm{near}} \exp\left(-\frac{\Delta r}{\lambda_\mathrm{near}}\right) + q_{0,\mathrm{main}} \exp\left(-\frac{\Delta r}{\lambda_\mathrm{main}}\right) \tag{5}$$

with 4 parameters: $q_{0,\mathrm{near}}$, $q_{0,\mathrm{main}}$, λ_near and λ_main. Δr is a distance from the LCFS. All the profiles were extracted from a single heat flux image during the plasma flat-top phase around $t \approx 1130$ ms. Results obtained by both cameras are quite consistent, however higher data points scatter is observed by the MWIR camera. It is probably caused by higher spatial resolution and sensitivity to hot spots thanks to the effect described above. This feature is evident mainly in the main-SOL, where the limiter was not cleaned by the plasma so well.

Comparison of the near and main-SOL contributions to the limiter heat load is described by the factor

$$R_q = q_{0,\mathrm{near}}/q_{0,\mathrm{main}}. \tag{6}$$

Plasma current dependence of the R_q is shown in Figure 6. Decreasing tendency of the near-SOL heat flux decay length λ_near with the plasma current and an opposite trend for the R_q coefficient is observed for both cameras.

Conclusion

The comprehensive study of radial profiles of the parallel heat flux in the COMPASS tokamak SOL has been performed. Results for a particular HFS limiter shape and insertion into the plasma, which

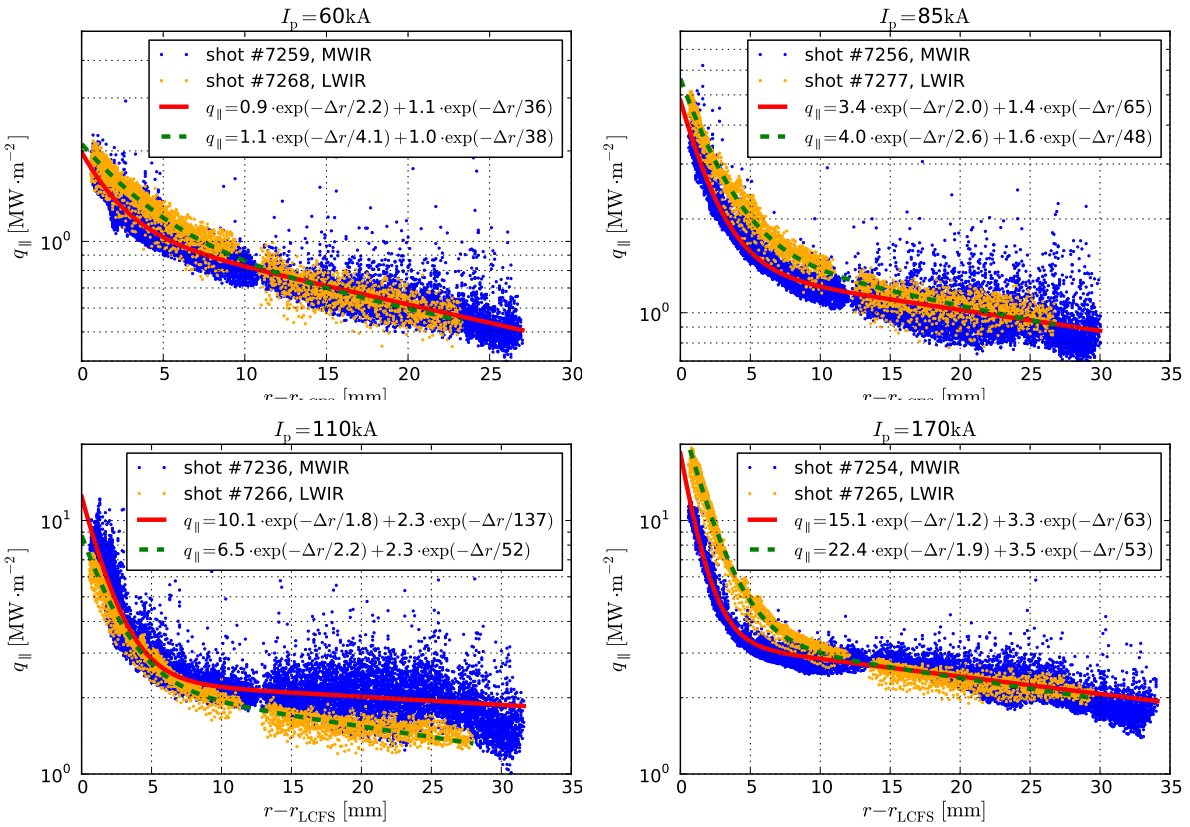

Figure 5. Radial profiles of the parallel heat flux in the SOL for 4 different plasma currents. Data from both MWIR and LWIR cameras are shown as well as double-exponential profile fits (5).

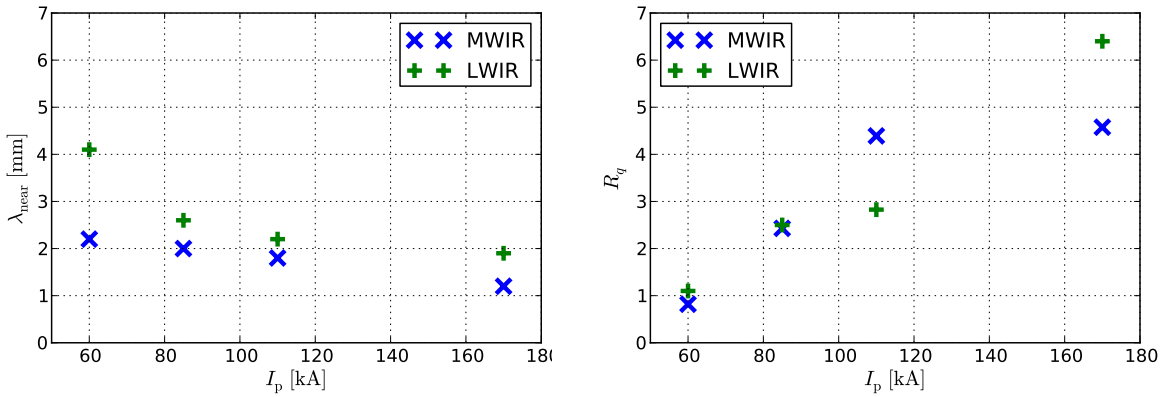

Figure 6. Left: near-SOL heat flux decay length for different plasma currents. Right: comparison of the near and main-SOL contributions to the limiter heat load depending on the plasma current.

represent the best approximation to the ITER case, have been presented in this paper. It has been demonstrated that the radial profile of the parallel heat flux in the SOL of HFS limited plasma measured by the means of both MWIR and LWIR cameras could be described by the double-exponential function. Resoulted narrow heat flux decay lenghts close to the LCFS scales inversely with a plasma current in accordance with the Heuristic drift-based model [*Goldston*, 2015].

Differences in MWIR and LWIR camera measurements were observed in accordance with previously published papers — particularly higher sensitivity of the MWIR camera to hot spots was encountered.

Acknowledgments. The work was supported in part by Grant Agency of the Czech Republic under Grant No. P205/11/2341 and MSMT Project No. LM2011021

References

Andrew, P., Coad, J., Eich, T., Gauthier, E., Herrmann, A., Matthews, G., Riccardo, V., and Stamp, M., Thermal effects of surface layers on divertor target plates, *Journal of Nuclear Materials*, *313–316*, 135–139, plasma-Surface Interactions in Controlled Fusion Devices 15, 2003.

Arnoux, G., Farley, T., Silva, C., Devaux, S., Firdaouss, M., Frigione, D., Goldston, R. J., Gunn, J., Horacek, J., Jachmich, S., Lomas, P. J., Marsen, S., Matthews, G. F., Pitts, R. A., Stamp, M., Stangeby, P. C., and JET-EFDA Contributors, Scrape-off layer properties of ITER-like limiter start-up plasmas in JET, *Nuclear Fusion*, *53*, 073 016, 2013.

Dejarnac, R., Stangeby, P. C., Goldston, R. J., Gauthier, E., Horacek, J., Hron, M., Kocan, M., Komm, M., Panek, R., Pitts, R. A., and Vondracek, P., Understanding narrow SOL power flux features in COMPASS limiter plasmas by use of langmuir probes, *Journal of Nuclear Materials*, pSI-21,P3-001, Manuscript submitted for publication, 2015.

Delchambre, E., Counsell, G., and Kirk, A., Effect of micrometric hot spots on surface temperature measurement and flux calculation in the middle and long infrared, *Plasma Physics and Controlled Fusion*, *51*, 055 012, 2009.

Delchambre-Demoncheaux, E., DeTemmerman, G., Loarer, T., Gauthier, E., Dunand, G., Gardarein, J., Kirk, A., Moncada, V., and Travere, J., Surface temperature measurement in the medium and long wavelength infrared range on MAST, *Journal of Nuclear Materials*, *415*, S1178–S1181, proceedings of the 19th International Conference on Plasma-Surface Interactions in Controlled Fusion, 2011.

Gauthier, E., Dumas, S., Matheus, J., Missirlian, M., Corre, Y., Nicolas, L., Yala, P., Coad, P., Andrew, P., and Cox, S., Thermal behaviour of redeposited layer under high heat flux exposure, *Journal of Nuclear Materials*, *337–339*, 960–964, PSI-16, 2005.

Goldston, R., Implications of the heuristic drift SOL model, *Journal of Nuclear Materials*, pSI-21, O-1, Manuscript submitted for publication, 2015.

Herrmann, A., Limitations for divertor heat flux calculations of fast events in tokamaks, in *ECA*, vol. 25A, pp. 2109–2112, 2001.

Herrmann, A., Thermal properties of plasma exposed carbon and heat flux calculations on a spatial scale of a few microns, *Journal of Nuclear Materials*, *337–339*, 907–911, pSI-16, 2005.

Herrmann, A., Junker, W., Gunther, K., Bosch, S., Kaufmann, M., Neuhauser, J., Pautasso, G., Richter, T., and Schneider, R., Energy flux to the ASDEX-Upgrade diverter plates determined by thermography and calorimetry, *Plasma Physics and Controlled Fusion*, *37*, 17, 1995.

Hildebrandt, D., Naujoks, D., and Sünder, D., Surface temperature measurements of carbon materials in fusion devices, *Journal of Nuclear Materials*, *337–339*, 1064–1068, pSI-16, 2005.

Horacek, J., Vondracek, P., Panek, R., Dejarnac, R., Komm, M., Pitts, R. A., Kocan, M., Goldston, R. J., Stangeby, P. C., Gauthier, E., Hacek, P., Havlicek, J., Hron, M., Imrisek, M., Janky, F., and Seidl, J., Narrow heat flux channels in the COMPASS limiter scrape-off layer, *Journal of Nuclear Materials*, pSI-21,O-4, Manuscript submitted for publication, 2015.

JEDEC, *Relative spectral response curves for semiconductor infrared detectors*, Electronic industries assoc., 1969.

Lott, F., Kirk, A., Counsell, G., Dowling, J., Taylor, D., Eich, T., and Herrmann, A., Thermographic power accounting in MAST, *Journal of Nuclear Materials*, *337–339*, 786–790, pSI-16, 2005.

Nespoli, F., Labit, B., Canal, G., Fasoli, A., Furno, I., and the TCV team, Heat loads in inboard limited l-mode plasmas in TCV, *Journal of Nuclear Materials*, pSI-21, P1-095, Manuscript submitted for publication, 2015.

Panek, R., Bilkova, O., Fuchs, V., Hron, M., Chraska, P., Pavlo, P., Stockel, J., Urban, J., Weinzettl, V., Zajac, J., and Zacek, F., Reinstallation of the COMPASS-D tokamak in IPP ASCR, *Czechoslovak Journal of Physics*, *56*, B125–B137, 2006.

Rogalski, A., *Infrared Detectors, Second Edition*, Taylor & Francis, 2010.

Stangeby, P. C., Lasnier, C., Tsui, C., Boedo, J., Elder, J., Kocan, M., Leonard, A., Makowski, M., McLean, A., Pitts, R., and Rudakov, D., Power deposition on the DIII-D inner wall limiter, *Journal of Nuclear Materials*, pSI-21, O-5, Manuscript submitted for publication, 2015.

Temmerman, G. D., Delchambre, E., Dowling, J., Kirk, A., Lisgo, S., and Tamain, P., Thermographic study of heat load asymmetries during MAST L-mode discharges, *Plasma Physics and Controlled Fusion*, *52*, 095 005, 2010.

Ulicny, J., *Calibration of infrared camera on tokamak COMPASS*, Bachelor thesis, Faculty of Nuclear Sciences and Physical Engineering, Czech Technical University in Prague, 2013.